Development of Compton Radiography Diagnostics for Inertial Confinement Fusion Targets

R. Tommasini, S. P. Hatchett, D. S. Hey, N. Izumi, J. A. Koch, O. L. Landen, A. J. Mackinnon, J. Delettrez, V. Glebov, C. Stoeckl

November 18, 2010

Disclaimer

This document was prepared as an account of work sponsored by an agency of the United States government. Neither the United States government nor Lawrence Livermore National Security, LLC, nor any of their employees makes any warranty, expressed or implied, or assumes any legal liability or responsibility for the accuracy, completeness, or usefulness of any information, apparatus, product, or process disclosed, or represents that its use would not infringe privately owned rights. Reference herein to any specific commercial product, process, or service by trade name, trademark, manufacturer, or otherwise does not necessarily constitute or imply its endorsement, recommendation, or favoring by the United States government or Lawrence Livermore National Security, LLC. The views and opinions of authors expressed herein do not necessarily state or reflect those of the United States government or Lawrence Livermore National Security, LLC, and shall not be used for advertising or product endorsement purposes.

Development of Compton Radiography of Inertial Confinement Fusion implosions

R. Tommasini, S. P. Hatchett, D. S. Hey, C. Iglesias, N. Izumi, J. A. Koch, O. L. Landen, A. J. MacKinnon, C. Sorce

Lawrence Livermore National Laboratory, Livermore CA

J. A. Delettrez, V. Yu. Glebov, T. C. Sangster, C. Stoeckl

Laboratory of Laser Energetics, Rochester NY

Abstract. An important diagnostic tool for inertial confinement fusion will be time-resolved radiographic imaging of the dense cold fuel surrounding the hot spot. The measurement technique is based on point-projection radiography at photon energies from 60-200 keV where the Compton effect is the dominant contributor to the opacity of the fuel or pusher. We have successfully applied this novel Compton Radiography technique to the study of the final compression of directly driven plastic capsules at the OMEGA facility. The radiographs have a spatial and temporal resolution of ~10 μm and ~10ps, respectively. A statistical accuracy of ~0.5% in transmission per resolution element is achieved, allowing localized measurements of areal mass densities to 7% accuracy. The experimental results show 3D non-uniformities and lower than 1D expected areal densities attributed to drive asymmetries and hydroinstabilities.

INTRODUCTION

In both direct and indirect drive [1], ignition can be spoiled by asymmetries in the laser or X-ray drive and hydrodynamic instabilities. An important tool to understand the reasons for possible failure or success will be time-resolved X-ray radiographic imaging of the dense cold fuel surrounding the hot spot. Indeed, images at stagnation time of the dense and cold deuterium-tritium fuel are fundamental to distinguishing between the various degradation mechanisms so they may be mitigated on the following attempts.

These images can be obtained using transmission Compton radiography [2,3], where we use high energy Compton scattering rather than traditional photo-absorption to cast a shadow of the imploding capsule. The Compton scattering cross section below and around 200 keV is largely independent of the probing photon energy [4] and density (we expect < 5% cross-section corrections for dense plasma degeneracy and strong
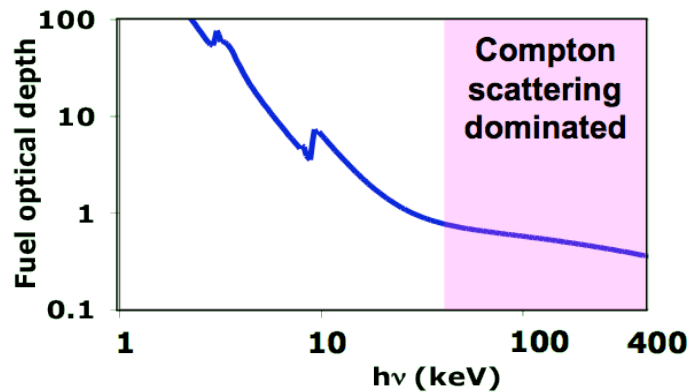
Figure 1: Optical depth of the fuel and ablator through center for a simulated NIF implosion.

coupling effects above 100 keV at up to the $3 \cdot 10^{26}/cm^3$ electron densities expected).

As a consequence, the optical depth of the fuel and ablator of a simulated ignition

attempt at the National Ignition Facility (NIF) [5], as seen in Figure 1, shows a plateau

above 50keV near an ideal value of 0.5, where the Compton scattering dominates the

net opacity.

The advantages of operating in the Compton-scattering regime are multiple. The use

of high-energy photons allows for filtering out the core self-emission, that, in the case

of NIF implosions is spectrally concentrated at photon energies below 30keV.

Integrating the probe photon energies over a large spectral region also means gaining

signal with respect to "monochromatic" Kα sources: typically factors of 10-20. The

relatively small variations of the total Compton cross section with respect to the probe

photon energy make the measurements based on Compton radiographs less sensitive

to any error in the spectrum of the probe photons. For instance, between 65 keV and

200 keV, corresponding to a 100% variation in the probe photon energy, the Klein-

Nishina cross section changes by only about 25%. Moreover since Compton scattering

is sensitive to electron density, and not to the atomic number, as in the case of the

photoelectric effect, it is ideal for probing the low-Z deuterium-tritium fuel in ICF

implosions. Short-wavelength photons will also minimize the refraction of the probing

X-ray beam as it traverses the shell and thus will keep the spatial resolution close to

the backlighter source size, Finally, by not requiring narrowband detection devices,

our technique greatly simplifies the experimental setup and apparatus. The energy

band of interest for the detected X-ray signal will be the convolution of a high pass

filter and the detector spectral response, and will be typically limited within 60keV-200keV photon energy region.

In this paper we report on the properties of high-energy, Bremsstrahlung, backlighters suitable as sources for Compton scattering based radiography, and on the application of this novel Compton Radiography technique to the study of the implosion of directly driven plastic capsules with different pressure fills of DD gas, near peak compression.

POINT PROJECTION RADIOGRAPHY USING BREMSSTRAHLUNG BACKLIGHTING SOURCES

Our scheme for the application of high-energy radiography on ICF implosions is based on point-projection radiography in the Compton scattering dominated regime.

Point-projection X-ray radiography offers many advantages: simplicity of alignment, use of small sources irradiated by intense short laser pulses to provide high spatial and temporal resolution, and option to use multiple sources to record the time history of fuel density and shape during the same implosion. It is important to note that in the case of radiography, the backlighter source is independently timed with respect to the implosion. In contrast other techniques such as down-scattered neutron imaging or spectrometry of charged fusion products are naturally synchronized with the neutron bang time and will only provide measurements averaged over time intervals of the order of the neutron burn time and with limited spatial resolution.

Moreover X-ray radiography does not require neutron yields, and can therefore be applied to experiments designed for tuning the implosion having low or no yield.

The downsides of X-ray radiography of ICF targets are related to the extreme background levels expected during the implosion. While the background associated with neutrons interacting with the detector can be eliminated using gating techniques, prompt background signals represent a formidable obstacle. These are mainly due to the X-rays emitted by the hot core, the hard x rays generated by hot electrons traversing the hohlraum walls, and the gamma rays from the n-gamma induced reactions in the various components inside the NIF target chamber. The spectra associated with these backgrounds extend from a few keV to a few hundred keV, therefore overlapping with the photon energy of any X-ray backlighting source. Assessing the backlighter performance, and their conversion efficiency in particular, is therefore crucial to estimating the signal that can be produced by the radiographic source.

The analysis of ICF simulated implosions on the NIF shows that spatial resolutions on the scale of 10 μm are needed in order to resolve small features in the cold dense fuel at peak compression. The same analysis shows that the requirements on the temporal resolution are less stringent, and while resolutions of the order of ~10 ps are desirable for recording radiographs of in-flight implosions, backlighter pulse durations of up to 100 ps are sufficient for radiographs of implosions at stagnation.

The backlighter of choice for the experiments described here consists of a 10 μm-diameter, 300 μm-long, Au wire. In most cases the wires are attached to 10 μm-thick, 300μm x 300μm, low-Z substrates. The wire is aligned along the radiography axis, i.e.

in a point-projection geometry.[6] This ensures that the object to be radiographed sees the Au wire end-on, therefore with an effective source size of the order of the wire diameter. Bremsstrahlung continuum radiation is generated by irradiating the Au micro-wires with short-pulse laser beams, producing intensities between 10^{17}-10^{18} W/cm^2 and having durations on the order of 10 ps.

In order to record the radiographs we designed and built a Compton Radiography Snout (CRS) consisting of a three-stage collimator, a layered structure of Al-Pb to shield against neutrons and high energy x and gamma rays, and a permanent magnetic field to deflect electrons away from the radiography line of sight. The CRS allows the insertion of filters at different locations, hosts an absolutely calibrated Fuji BAS imaging plate detector at about 400 mm from target chamber center, and features a built-in step-wedge filter/collimator that allows the reconstruction of the
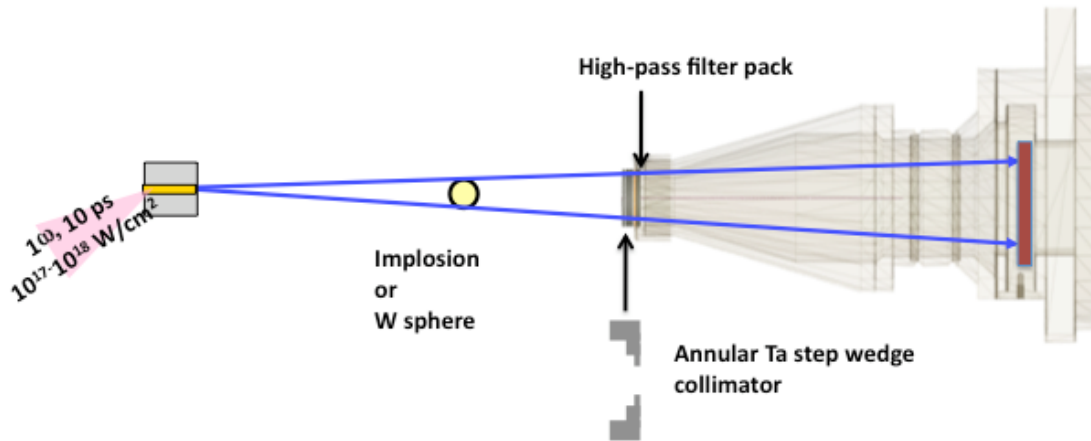
Figure 2: Experimental setup to obtain 2D high X-ray energy radiographs. The short pulse beam drives an Au micro-wire on a low-Z substrate. The radiograph is recorded on absolutely calibrated imaging plates. An annular Ta step wedge, is used to measure the continuum spectrum along the radiography axis, while the high-pass filter combined with the imaging plate quantum efficiency provides the spectral discrimination of the X-rays producing the radiograph.

Bremsstrahlung spectrum along the line of sight. A combination of high- and low-Z filters is used inside the snout as a high-pass X-ray energy filter. This, together with the imaging plate quantum efficiency, provides the spectral discrimination of the X-rays producing the radiograph.

Figure 2 shows the experimental setup we have used at the TITAN laser facility at LLNL (Livermore, CA) and at the OMEGA and OMEGA EP laser facilities at LLE (Rochester, NY). [7]

This setup allows us to record radiographs and the X-ray spectrum simultaneously in line with the radiography axis. In some shots, a 200-µm diameter tungsten-carbide sphere replaces the capsule in order to check the spatial resolution in all directions.

Other diagnostics we have routinely used during the experiments are: an ultrafast X-ray streak camera, to measure the backlighter pulse duration, and therefore the temporal resolution of the radiographs, and a neutron streak camera, to measure the neutron peak burn time and duration.

REFRACTION BLUR IN HIGH ENERGY POINT-PROJECTION X-RAY RADIOGRAPHY OF ICF TARGETS

In point-projection X-ray radiography, using photons with high energy helps to minimize the refraction of the probing X-ray beam as it traverses the shell and thus to keep the spatial resolution close to the backlighter source size. The blur in source size due to refraction of the X-ray beam as it traverses the imploding shell can be estimated
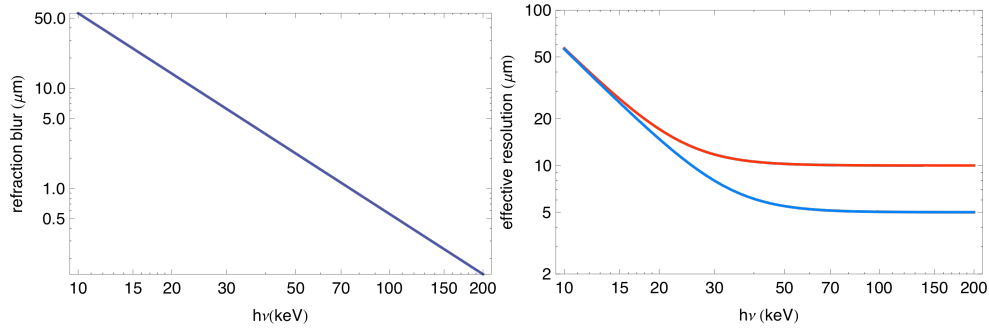
Figure 3: a) Additional refractive blur contribution as function of probe photon energy for expected ICF implosion conditions the NIF; b) Effective resolution as function of probe photon energy for 5 and 10 μm source sizes.

as follows: defining Δx as the gradient scale-length for the electron density, the refraction angle of a X-ray traversing the imploding fuel along a chord of length L is given by $\phi = L \, \Delta\eta/\Delta x$, where $\Delta\eta$ is the refractive index differential. The apparent blurring of a point source at distance p from the imploding fuel will therefore be: $\sigma_b = p \, \phi = p \, (L/\Delta x) \, n_e/(2 \, n_c)$, where we have used the free electron refractive index differential $\Delta\eta \cong n_e/(2 \, n_c)$ in the expression for ϕ, applicable for photon energies well above any ionization potentials. In a converged capsule we typically have $L \cong 4\Delta x$, so that we can write $\sigma_b = 2 \, p \, n_e/n_c$.

Substituting the expression for the critical density, $n_c = 1.1 \; 10^{21} \, \lambda^{-2}/cm^3 \approx 7.2 \; 10^{26}$ $h\nu^2/cm^3$, with the photon energy $h\nu$ expressed in keV , we get the simple equation: σ_b (in cm) $= 2.8 \; 10^{-27} \, n_e \, p \, / \, h\nu^2$, with the electron density in $1/cm^3$ units. Assuming a typical mass density of 800 g/cm^3 [1] for a NIC implosion, corresponding to $n_e \sim 2$ $10^{26}/cm^3$, and assuming 1 cm distance BL-shell, we plot for the refractive blur in Figure 3a, and effective resolution in Fig 3b assuming source sizes of 10um and 5um respectively. Figure 3b shows that refraction blur becomes negligible (<10% degradation in resolution) above 35 keV and 50 keV, respectively.

The loss in resolution can be quantified in the alternate way: we define the fractional

loss in resolution as $f = \left(\sigma^2 + \sigma_b^2\right)^{1/2}/\sigma - 1$, where the backlighter resolution is

indicated by σ. Taking the first order Taylor expansion and substituting the σ_b

expression above gives: $f = \dfrac{(2n_e)^2}{h\nu^4}\left(\dfrac{p}{\sigma}\right)^2$, therefore valid as long as $f \ll 1$, with n_e in

units of $10^{27}/\text{cm}^3$, hν in keV and f in μm. Solving for the photon energy gives

$h\nu = \dfrac{(2n_e)^{1/2}}{f^{1/4}}\left(\dfrac{p}{\sigma}\right)^{1/2}$, which gives the value for the probe photon energy corresponding

to a fractional loss in resolution of f, note that p can be conveniently expressed in

backlighter resolution units, σ. For our experimental geometry (p ~ 1 cm, n_e = 0.2

$10^{27}/\text{cm}^3$), allowing < 10% loss in resolution, leads to hν > 35 keV and hν > 50 keV

for σ = 10 μm and σ = 5 μm, respectively, in agreement with Fig. 3b.

ROLE OF THE SUBSTRATE IN MICRO-WIRE

BACKLIGHTERS

While a substrate is not required in principle to hold the Au micro-wires producing the

backlighter source, its presence might in some cases be required by the experimental

conditions. In some facilities the substrate might be required to ease pointing of the

short pulse beam onto the backlighter. In some other facilities the substrate might be

required to avoid any transmission of the short pulse laser energy through the target.

In order to understand the consequences of the substrate onto the quality of the

radiographs, we performed experiments on TITAN, employing Au micro-foils, 10 μm

thick, Au micro-wires on Al and CH substrates, as well as freestanding Au micro-wires, with the experimental setup shown Fig.2.
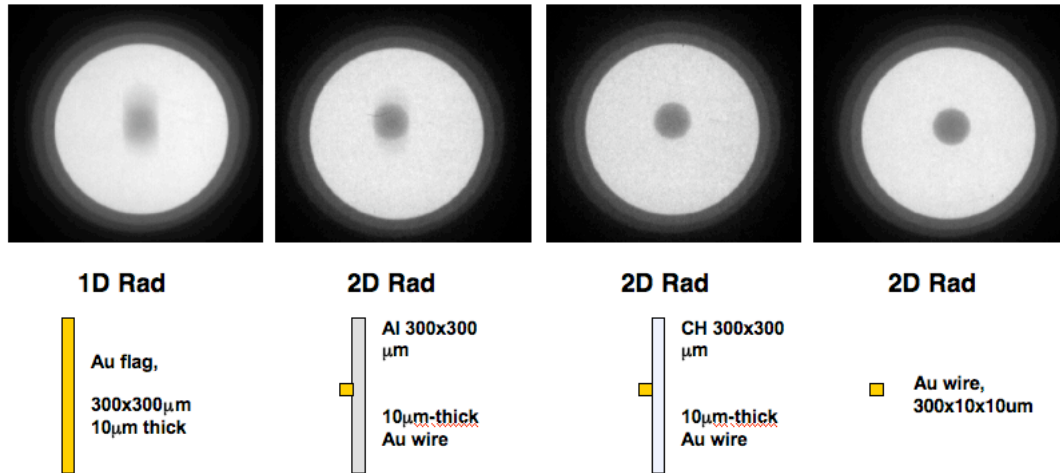

Figure 4: Radiographs of solid tungsten-carbide spheres obtained using different types of backlighters shown below. Also seen is the transmission through annular Ta step wedge at the edges of field-of-view.

The TITAN short pulse laser beam was used to irradiate the targets with an angle of ~70 degrees with respect to the surface and with a spot size of about 50 μm, a pulse duration of 10 ps and energy on target of about 200 J. Figure 4 shows the radiographs of the solid tungsten-carbide spheres, 200um diameter, obtained using the different types of backlighters. The Al-substrate is causing an undesirable secondary radiograph of the tungsten-carbide sphere, similar to the 1D radiograph obtained using a Au foil, superimposed onto the 2D radiograph from the Au wire. As expected, given the lower Z and density of the substrate with respect to Al, the CH substrates give no discernible secondary radiograph. Freestanding wires give the cleanest 2D radiographs. In the rest of this article, we will only refer to backlighters made of 10-μm -diameter, 300-μm-long Au wires, on 10-μm-thick CH substrates.

CHARACTERIZATION OF MICRO-WIRE BREMSSTRAHLUNG BACKLIGHTERS FOR HIGH ENERGY POINT PROJECTION RADIOGRAPHY

Using the setup shown in Figure 2, we have performed experiments to characterize the properties of Au micro-wire backlighters. The experiments have been performed at the OMEGA and OMEGA EP laser facilities of LLE (University of Rochester, NY) and at the TITAN laser facility of LLNL (Livermore, CA). Short-pulse backlighters were produced using the 1ω laser beam of OMEGA EP and TITAN, 10 ps long, with nominal intensities on target in the 10^{17}- $4x10^{18}$ W/cm^2 range. Longer-pulse backlighters were produced overlapping up to 18, 3ω laser beams of OMEGA, 100 ps long, with nominal intensities on target in the $3x10^{16}$- 10^{17} W/cm^2 range. This configuration is of interest as it represents the earliest available option for implementing Compton radiography on the NIF, and will be discussed in the last section of this article. The conversion efficiency of the backlighters, into 70-200 keV X-rays, was measured fitting a Bremsstrahlung spectrum to the data from the annular step-wedge filter of the CRS. As shown in Figure 5, we have consistently measured conversion efficiencies between 2e-4 to 8e-4 in the 10^{17}-$4x10^{18}$ W/cm^2 intensity range, and between 1e-5 and 3e-5 for the 1ω and 3 ω case, respectively. The Bremsstrahlung spectra show typical electron temperatures of ~150-250 keV, for 1ω-10ps produced backlighters, and ~50–90 keV for 3ω-100ps laser-produced backlighters. Our measurements of X-ray yield also show that the freestanding wires perform as well as the wires on substrates, in terms of X-ray yield.

The source size of the backlighters were measured by fitting simulated radiographs obtained with different Gaussian sources sizes, and using the spectra measured by the CRS step-wedge, to the experimental radiographs of tungsten-carbide spheres. Figure 6 shows the results for two particular shots. This method resulted in typical source sizes of (11 ± 2) µm and in all cases close to the diameter of the Au wires. The measurements of pulse durations were carried over at the OMEGA and OMEGA EP laser facilities using an X-ray streak camera and measuring the emission from Au in the spectral region above 3keV. Figure 7 shows the results for two
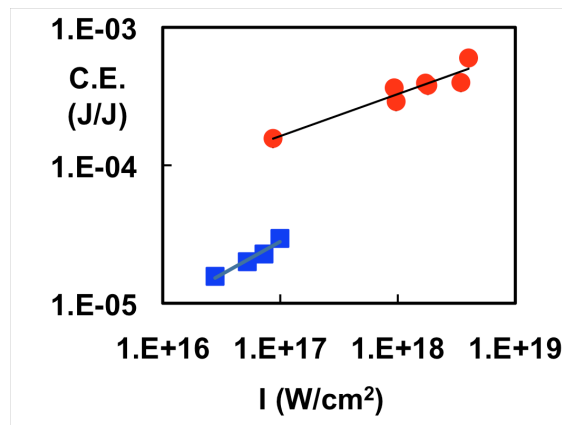

Figure 5: Conversion efficiency as a function of laser intensity into 70-200 keV X-rays from 1ω-10ps (dots) and 3ω-100ps (squares) laser-produced Au micro-wire backlighters.

particular cases, corresponding to 12 ± 3 ps and 100 ± 5 ps, for 1ω-10ps produced backlighters, and for 3ω-100ps laser-produced backlighters, respectively. In all cases we have observed that the X-ray pulse duration closely follows the duration of the laser pulse.
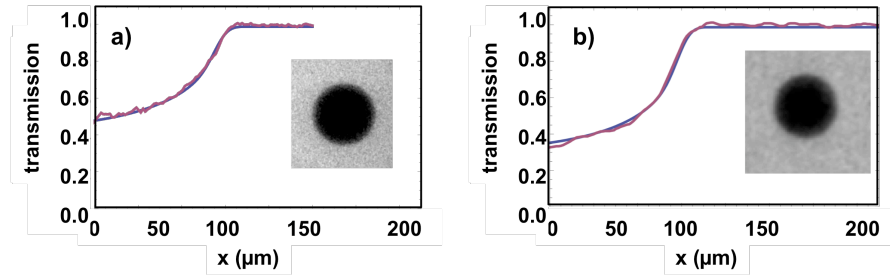
Figure 6: 2D Radiographs and lineouts from backlit 200 µm-diameter solid tungsten-carbide spheres for a), 1ω-10ps,.and b) 3ω-100ps cases. Blue (Purple) lines are data and 2D simulated radiographs assuming 11 µm FWHM source size.
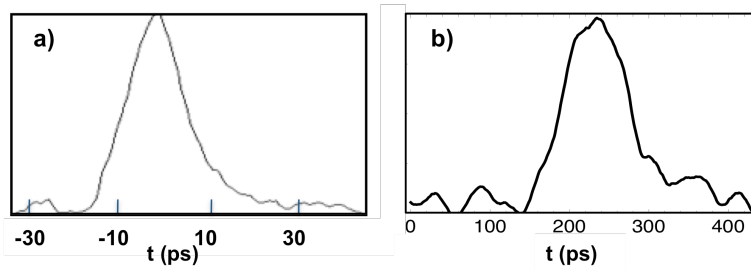
Figure 7: X-ray temporal profiles from a) 1ω-10ps, and b) 3ω-100ps laser-produced Au micro-wire backlighters as measured by X-ray streak camera.

OMEGA/OMEGA-EP INTEGRATED EXPERIMENTS: DEMONSTRATION OF COMPTON RADIOGRAPHY OF IMPLOSIONS

Here we describe the application of Compton Radiography to compare the compression of spherical implosions with different pressure fills.
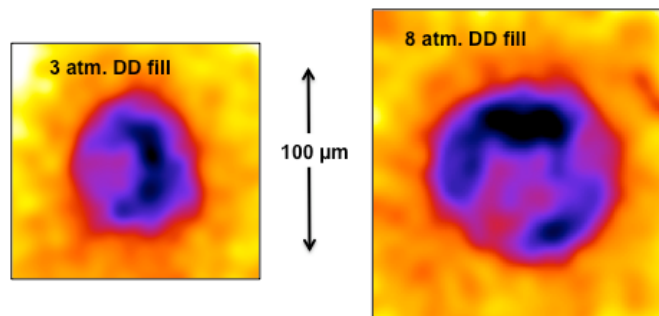

Figure 8: Compton Radiographs of CH imploding shells obtained at OMEGA/OMEGA-EP. Left: radiograph of a 3atm-DD-filled CH shell, at about 50ps from peak compression, obtained at a photon energy of ~60keV. Right: radiograph of a 8atm-DD-filled CH shell, within 20ps from peak compression, obtained at a photon energy of ~100keV.

For these experiments we used 60 beams of the OMEGA laser facility for direct-drive implosions of 40μm thick, 870μm diameter CH capsules filled with 3atm and 8atm DD gas, located at the target chamber center (TCC) of OMEGA. As a backlighter we used a 10 μm diameter Au wire, 300 μm long, in a point-projection, end-on, geometry at 10 mm distance from TCC. The backlighter was driven by the OMEGA EP short pulse beam, delivering ~1kJ at 10ps in a 100um square spot size. The time delay between the OMEGA EP short pulse and the OMEGA laser pulses was chosen to

capture the time of peak compression predicted by the 1D radiation hydrocode LILAC,[8] however a perfect timing was not possible due to a ± 25 ps temporal jitter between the EP short pulse beam and the OMEGA driver beams. The radiographs were recorded using the CRS at 38x magnification. Figure 8 shows the radiograph of a 3atm-DD-filled CH shell (left), at 50 ± 25 ps prior peak compression and the radiograph of a 8atm-DD-filled CH shell (right), at 20 ± 25 ps past peak compression. The statistical accuracy of these radiographs is very good: ±0.5% in transmission in the unattenuated regions, corresponding to about 40000 detected photons / resolution
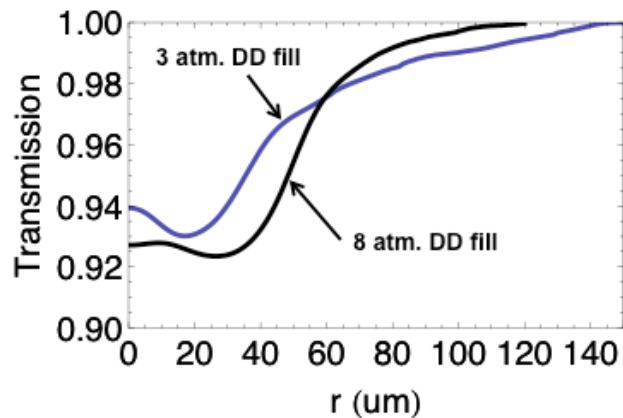

Figure 9: Azimuthally averaged radial lineout of transmission for the Compton radiographs from Fig. 8.

element. As discussed in the previous sections, the spatial and temporal resolutions are ~ 10 μm and 10 ps, respectively. The radiographs show expected limb darkened profiles and smaller size for lower fill. Figure 9 shows the azimuthally averaged transmission lineouts of the Compton radiographs from Fig. 8. The average diameters measured from the radiograph are 80 μm and 100 μm, respectively, The transmissions

for the two different DD fills are not directly comparable as the radiographs have been obtained using different X-ray probe spectra, i.e. at average photon energies of 60 keV and 100keV, respectively. To provide a comparison with 1D simulations we have applied an Abel inversion on the azimuthally averaged transmission profiles to calculate the mass density and the areal density $\rho\Delta R$ of the implosions. This procedure results in $\rho\Delta R$ values of 190 ± 13 mg/cm^2 and 222 ± 16 mg/cm^2, for the 3 atm DD fill and the 8 atm DD fill, respectively. Figure 10 shows the comparison with the corresponding values derived from 1D simulations, including the effect of 10 μm resolution. We can see that the areal densities measured by radiography are below the 1D predicted values, at the 62% and 75% level, for 3 atm. and 8 atm. fill, respectively. Note that, while from both first principles and 1D simulations, one should expect higher peak areal densities for the lower fill capsules, the radiographs reveal that the shell having higher fill pressure achieves in practice larger areal densities. By contrast, the measured total mass remaining in a field of view having a radius of 140 μm reaches the values of 56 ± 5 μg and 55 ± 5 μg, for 3 atm. and 8 atm. fill, respectively. Since mass values (scaling as $\rho\Delta RR^2$) are only 10% lower than the corresponding 1D predicted values, while $\rho\Delta R$ values are $\approx 30\%$ lower, this would indicate that the 1D simulations are predicting $\approx10\%$ smaller implosion size R at the nominal times of the radiographs. Indeed 1D simulations predict 10% smaller diameters than measured from the radiographs. We ascribe the deviation from the 1D predictions to 3D nonuniformities as seen in the images due to asymmetries in the laser drive or hydrodynamic instabilities.

This aspect can be fully appreciated by analyzing the chord-integrated density maps.
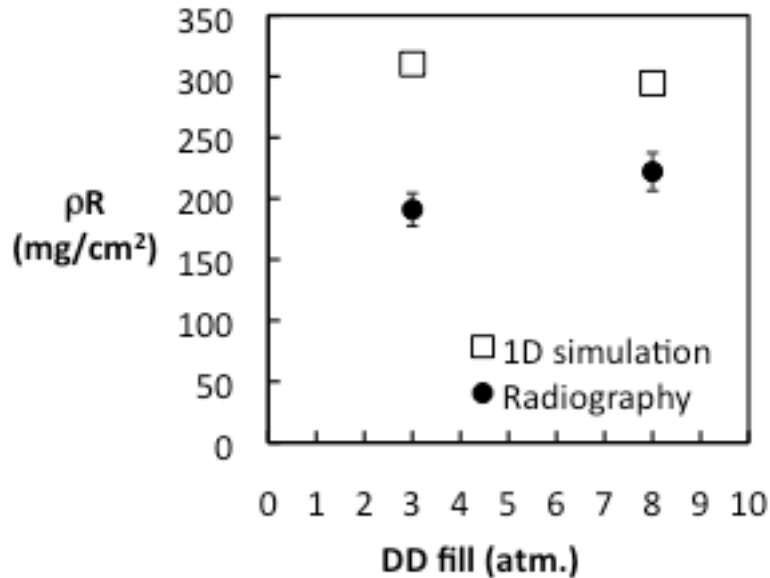

Figure 10: Areal densities of plastic shell implosions vs DD fill: comparison between values from 1D simulations and values measured from Compton radiographs.

Defining L as the one half the chord length, ρL is then the areal density integrated along this chord. This quantity is calculated directly form the 2D transmission radiographs according to the equation: $\rho L(x,y)=Log[1/T(x,y)]/(2\ \mu_C)$ where T is the transmission and μ_C the Compton cross section in units of cm^2/g.

Figure 11 shows the 2D ρL maps for the two cases. The maps clearly carry over the asymmetries evidenced by the Compton radiographs and show a larger, more uniform and symmetric implosion in the case of the 8 atm. fill. ρL reaches peak values of 240 mg/cm^2 and 300 mg/cm^2 along the limb, for the 3 atm. and 8 atm. fill pressure cases, respectively. We finally want to point out that, in contrast to the Abel inversion of

azimuthally averaged transmission profiles, the ρL plots have the advantage of being
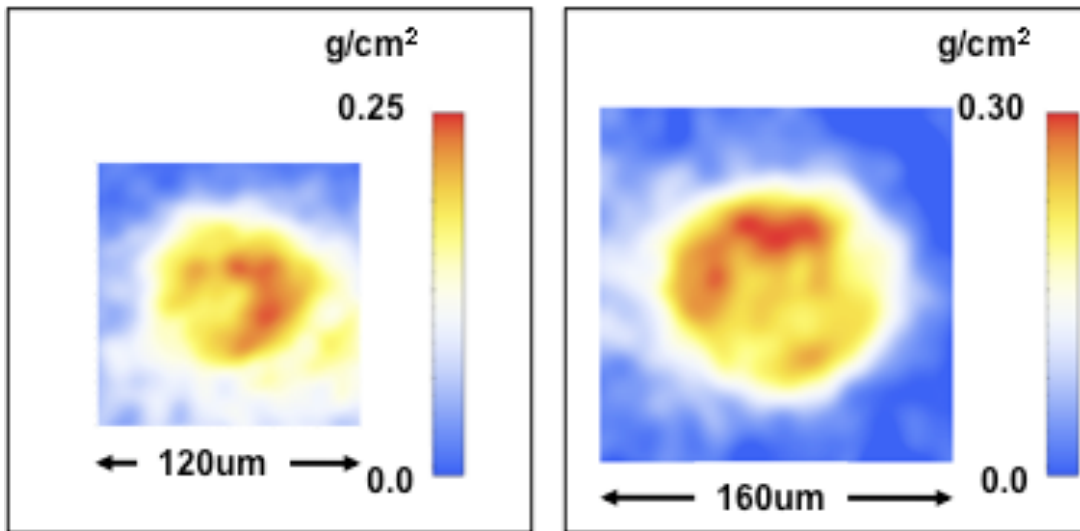
Figure 11: 2D ρL maps for the 3 and 8 atm-fill cases

free of the systematic error related to defining the radiograph centroid.

IMPLEMENTATION OF COMPTON RADIOGRAPHY ON THE NIF

As seen in a previous section, Au micro-wire Bremsstrahlung backlighters generated by 3ω laser pulses of about 100 ps pulse duration, are capable of conversion efficiencies in excess of 1E-5, into 70 keV to 200 keV continuum, with source sizes matching the wire diameter, i.e. 10 μm, and lifetimes matching the laser pulse durations. This option is extremely attractive for the immediate implementation of Compton Radiography on the NIF.

Indeed, in the first instance the backlighting source will be produced by irradiating 2 Au wires with the UV beams from two NIF quads (8 beams total, 4 per wire) independently timed. Given a peak power/beam of 2 TW for short pulses (< 1 ns) and minimum spot size of 250 μm, this will produce an intensity of 1-2e16 W/cm^2. The setup is shown in Figure 12. Collimation to avoid multiple exposures will be added on the backlighter side, at the hohlraum wall.

The main concerns for recording Compton radiographs of the fuel are related to the extreme background levels expected during the implosion. The radiographs will be recorded by a Gated X-ray Imager (GXI) that consists of a micro-channel plate coupled to a framing camera, with gate times adjustable within the 30-200 ps range. [9,10] It has recently been demonstrated to provide gated images even at 100 keV

which volumetrically excite the MCP. The gating will mitigate the background associated to later arriving neutrons and gamma rays from the n-gamma induced reactions in the various components inside the NIF target chamber. A combination of further collimators will reduce the background from hard X-rays generated by hot electrons traversing the hohlraum walls and, if necessary, from gamma rays from n-gamma induced reactions in nearby mass. Using a high-pass filter, coupled to the detector spectral response, we will limit the recorded X-ray photon energy to 60 keV-200 keV, to reduce the background from the X-rays emitted by the hot core.

The use of multiple Au wires in a predefined temporal sequence will provide multiple snapshots of the cold fuel through stagnation time. These radiographs will allow 2D reconstruction of the fuel density and shape.

The accuracy of measurements of fuel areal density depends essentially on the signal-to-noise ratio and on the contrast of the recorded radiograph. Using the conversion efficiency of 1e-5 from Fig. 5 and assuming a gate time of 70 ps, we expect signals of the order of a few hundreds photons per resolution element of signal, providing 10% or better accuracy in ρL per resolution element. Figure 13 shows a 10um/70ps, spatial/temporal resolution, Compton radiograph of a NIF driven implosion (a)
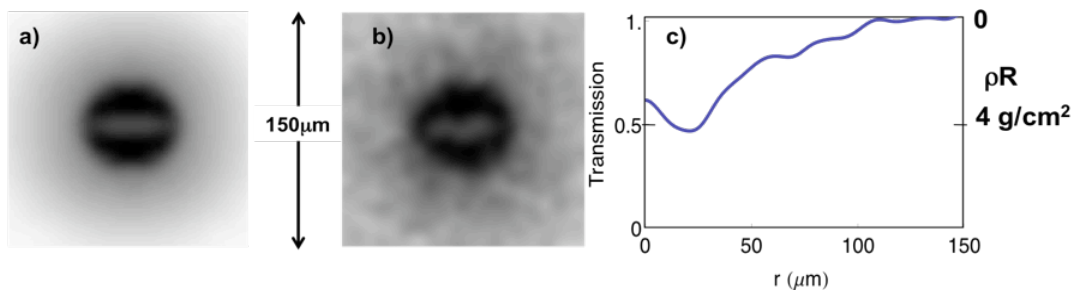
Figure 13: a) simulated Compton radiograph of a NIF driven implosion including 10um/70ps, spatial/temporal resolution; b) including noise expected when using NIF UV beams to generate the backlighter; c) transmission profile along the vertical diameter.

together with the same radiograph including the noise expected when using NIF UV beams to generate the backlighter (b). The transmission profile along the vertical diameter (c) shows expected 50% contrast.

When the short pulse capability is available on the NIF [11], 10 ps, 1 kJ/beam pulses can be used to irradiate the Au micro-wires, for which expect 2% statistical accuracy and improved temporal resolution.

CONCLUSIONS

We have defined the experimental setup for hard X-ray radiography of ICF implosions. The scheme is based on point-projection radiography in the Compton scattering dominated regime for the opacity of the fuel or pusher.

We have successfully applied this novel Compton Radiography technique to the study of the compression of plastic capsules with different pressure fills of DD gas, near peak compression, by recording high spatial (10 μm) and temporal (10 ps) resolution radiographs. The radiographs allow measurements of areal densities and masses with 5 – 10% accuracy. The average areal densities and radii are less and more than predicted by 1D simulations, respectively, and combined with the 3D non-uniformities observed provide quantitative evidence of the effects of residual drive asymmetries and/or hydroinstability growth.

ACKNOWLEDGMENTS

REFERENCES

1. J. D. Lindl et al., Phys. Plasmas **11**, 339 (2004)

2. R.Tommasini et al., Atomic Processes in Plasmas, American Institute of Physics, 2007, pp. 248 - 255.

3. R.Tommasini et al., REVIEW OF SCIENTIFIC INSTRUMENTS **79**, 10E901   2008

4. Klein, O; Nishina, Y, Z. F. Phys. 52: 853 and 869 (1929).

5. G. H. Miller, E. I. Moses, and C. R. Wuest, Nucl. Fusion **44**, S228 (2004)

6. Park HS, et al., Phys. Plasmas **13**, 056309 (2006)

7. T. R. Boehly *et al*., Opt. Commun. **133**, 495 (1997)

8. J. Delettrez *et al*., Phys. Rev. A **36**, 3926 (1987)

9. J. D. Kilkenny, Laser Part. Beams **9**, 49   1991,

10. N. Izumi et al., REVIEW OF SCIENTIFIC INSTRUMENTS **81**, 10E515   2010

11. J. K Crane et al. Journal of Physics: Conference Series **244** 032003 (2010)